AD-A088 369 TEXAS UNIV AT AUSTIN APPLIED RESEARCH LABS F/G 20/1
SIGNAL PROCESSING ASPECTS OF NONLINEAR ACOUSTICS.(U)
JUL 80 T G MUIR, T G GOLDSBERRY N00014-75-C-0161
UNCLASSIFIED ARL-TR-80-38 NL

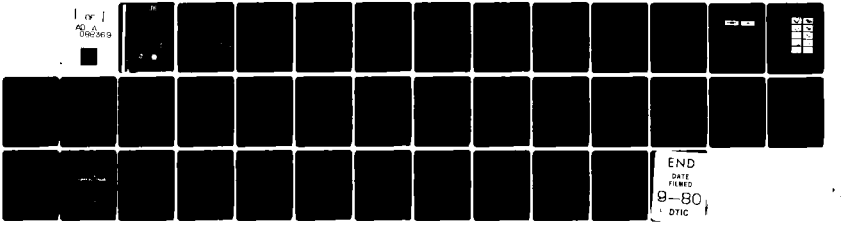

(12) LEVEL II

ARL-TR-80-38

Copy No. 110

SIGNAL PROCESSING ASPECTS OF NONLINEAR ACOUSTICS

T. G. Muir
Tommy G. Goldsberry

APPLIED RESEARCH LABORATORIES
THE UNIVERSITY OF TEXAS AT AUSTIN
POST OFFICE BOX 8029, AUSTIN, TEXAS 78712

7 July 1980

Technical Report

APPROVED FOR PUBLIC RELEASE;
DISTRIBUTION UNLIMITED.

Prepared for:

OFFICE OF NAVAL RESEARCH
DEPARTMENT OF THE NAVY
ARLINGTON, VA 22217

SIGNAL PROCESSING ASPECTS OF NONLINEAR ACOUSTICS

by

T. G. Muir and T. G. Goldsberry

Applied Research Laboratories
The University of Texas at Austin
Austin, Texas 78712

Prepared for:

Office of Naval Research
Contract N00014-75-C-0161

This paper has been submitted by invitation to the NATO Advanced Study Institute on Underwater Acoustics and Signal Processing, Copenhagen, Denmark, 18-29 August 1980.

SIGNAL PROCESSING ASPECTS OF NONLINEAR ACOUSTICS

T. G. Muir and T. G. Goldsberry

Applied Research Laboratories
The University of Texas at Austin
Austin, Texas 78712

1. INTRODUCTION

The topic of nonlinear acoustics has been included at previous NATO study institutes going back to 1966. The first treatment, by Berktay (1), speculated on the possibilities nonlinear effects might offer. In 1968, Mellen (2) illustrated some of these possibilities through laboratory tank experiments. Berktay returned in 1972 (3) to present some engineering models for the design of parametric sources. In 1976, Bjørnø (4) presented a survey of theoretical and experimental results on parametric arrays developed at several laboratories.

Today, research and development in nonlinear acoustics has gravitated toward applications. The present paper therefore addresses applications with a view towards outlining the unique features of nonlinear arrays, especially with regard to signal processing. Both nonlinear sources and receivers will be discussed.

As research tools, nonlinear sources offer a means of quantifying both the limitations of the medium as well as the payoffs of new approaches and techniques. In the following pages, we will illustrate this claim through presentation of results obtained with several nonlinear research tools configured for model tests as well as full-scale experimentation.

Parametric receivers also have potential as research tools but they are of interest primarily for their application as both fixed and mobile sensors, pending the successful development of practical signal processing techniques.

2. NONLINEAR SOURCES

As is well known, nonlinear sources create highly directive sound through the nonlinear interaction of intense radiations that are themselves directive. Parametric interaction of two high frequency waves yields difference frequency waves, while the distortion and/or self-interaction of a single frequency wave leads to the creation of harmonic radiations. Difference frequency radiations have the advantage of low frequency, high directivity, and wide bandwidth, all realized from a relatively small primary source. There is a disadvantage of low conversion efficiency. Much of the conversion loss from primary to difference frequency sound can be made up by signal processing gains, as will be subsequently discussed. Harmonic radiations have the advantage of high directivity, wide bandwidth, and good conversion efficiency, with the disadvantage of high frequency that is prone to absorption by the medium.

Those not familiar with nonlinear acoustics may find one of the tutorial or review articles useful (4,5).

2.1. Directivity of Parametric Sources

The beamwidth capability of the parametric array has as a theoretical limit the Westervelt result (6),

$$\theta_{HP} = 4\sqrt{\frac{\bar{\alpha}}{k_s}} \qquad (1)$$

where θ_{HP} is the half-power beamwidth, $\bar{\alpha}$ is the mean absorption coefficient of the primaries, and k_s is the difference frequency wave number. Here we see that the lower the absorption, the longer the array and the greater the directivity of the parametric radiation.

Eq. (1) is shown graphically in Fig. 1 for a downshift ratio of ten (primary frequency $f_p \div$ difference frequency f_s). Actually, the directivity function of a parametric array is the convolution of the product of the primary directivity functions, $D_p(\theta)$, with the Westervelt end-fire array directivity (5), $D_w(\theta)$, weighted by $\sin\phi$, i.e.,

$$D_s(\theta) = \int D_p(\phi)\, D_W(\theta-\phi)\, \sin\phi d\phi \quad , \qquad (2)$$

where θ is the observation angle measured from the acoustic axis, ϕ is the angle variable (to an annulus of integration about the acoustic axis), and

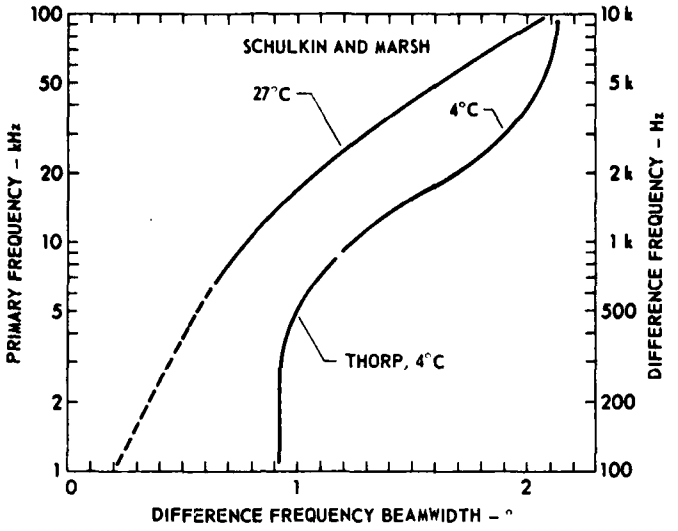

Figure 1. Farfield beamwidth capability for a parametric array having a downshift ratio of 10, as predicted from the Westervelt formula, using seawater absorption data as indicated.

$$D_W(\theta-\phi) = \left[i\,\bar{\alpha} + k_s \sin^2\left(\frac{\theta - \phi}{2}\right)\right] \quad . \tag{3}$$

Since the convolution effect accounts for broadening of the parametric directivity due to the finite size of the primary beams, the Westervelt directivity, Eq. (1), and the corresponding plot of Fig. (1) can only be approached as a limit. It can nonetheless be seen that warm water permits smaller beamwidths than cold water (Shulkin and Marsh absorption data) while consideration of the boron-borate relaxation process (Thorp data) (7) leads to practically constant parametric directivity below about 5 kHz. If maximum parametric directivity is desired, primary frequencies near 5 kHz appear optimum.

2.2. Applications of Directive Parametric Devices

Possession of a narrow system beamwidth with good minor lobe suppression enables one to reject environmental backscatter and improve echo-to-reverberation ratios, E/R. Usually, improved E/R increases detection probability, although just being able to detect the target often provides classification clues, as is the case in Doppler measurements. Extremely narrow beamwidths are useful in acoustic imaging, which enables the classification of targets as to size and shape.

We argue here that these capabilities are equivalent to signal processing capabilities since the same goals are achieved

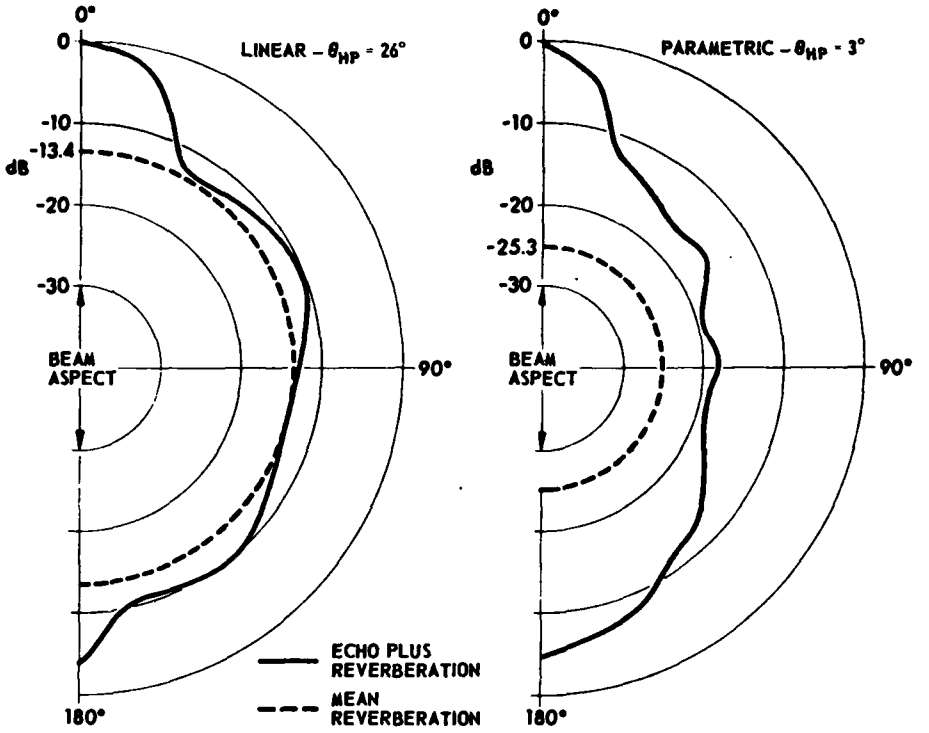

Figure 2. Scattering patterns from a model submarine.

in both cases. We therefore have signal processing upon transmission with a directive nonlinear source.

2.2.1. Model submarine experiments. An example of the utility of the high directivity of the parametric array in sonar research is offered by the data of Fig. 2. Here we see some normalized scattering patterns from a model submarine some 2 m in length that were acquired with the target placed in rotation at mid depth in a shallow water lagoon. The water was 1.4 m deep, overlaying a sand bottom. The range was 250 m, and the signal was a 3.5 msec cw ping at 15 kHz. Two patterns are shown. One is for a linear radiation from an array 23 cm in diameter with a half-power beamwidth of 26°. The other was acquired with a parametric array developed from primaries centered at 225 kHz and emitted through the same sized aperture to develop a parametric beam 3° wide. As expected, the broad beam linear system insonifies much more of the backscattering surfaces and volume scatterers, to the extent that the target is really only detected near beam aspect. The narrow beam parametric system insonifies fewer scatterers and the mean reverberation is suppressed by 11.9 dB over that of the linear system. Simple theory, based solely on insonified area, would predict a suppression of 8.2 dB.

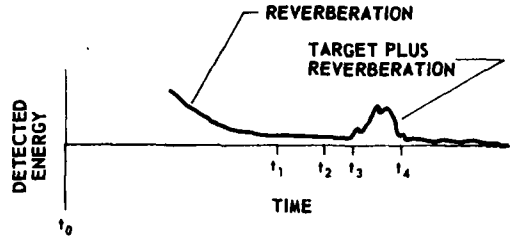

Figure 3. Signal envelope for model submarine echo data.

As can be seen, the 3° parametric beam has sufficient E/R to detect the target at practically all aspects.

It is instructive to use the experimental data to determine the detection probability of the model target as a function of detection threshold. The latter is defined for a 50% false alarm rate as

$$D = \frac{T - B}{\sigma_B} \quad , \tag{4}$$

where

$T = \int_{t_3}^{t_4} V_r^2(t)\, dt$, the target plus reverberation energy in each echo,

$B = \left\langle \int_{t_1}^{t_2} V_r^2(t)\, dt \right\rangle_{ensemble}$, the reverberation only signal, and

$\sigma_B^2 = \left\langle \int_{t_1}^{t_2} \left[V_r(t)-B\right]^2 dt \right\rangle_{ensemble}$, the variance of reverberation energy,

where $V_r(t)$ is the received signal and the times t_i are shown in Fig. 3. One computes B and σ_B^2 as constants from the data ensemble and then computes the probability of observing the target as the ratio of number of times each measured D exceeds a given D_x to the number of estimates in the ensemble, i.e.,

$$\text{Probability}\left[D_i > D_x\right] = \frac{n_{D_i > D_x}}{N} \quad . \tag{5}$$

The narrowbeam parametric system achieved a 95% detection probability at a 0 dB threshold, compared to 50% for the broadbeam

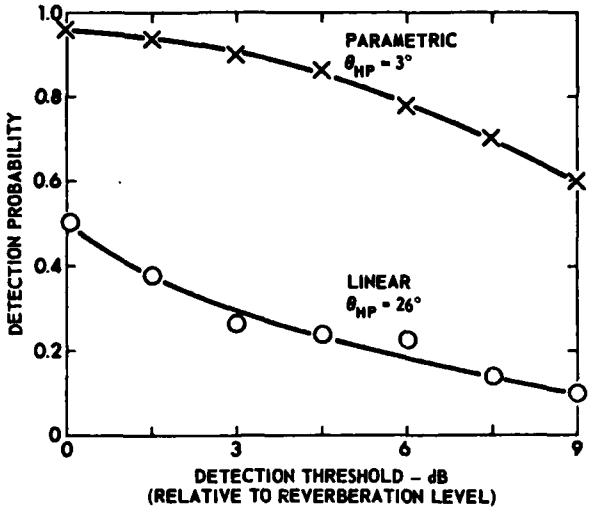

Figure 4. Detection probability for model submarine echo data.

case; the results are shown in Fig. 4. With increase in threshold, the detection probability of the narrowbeam system falls off slower than for its broadbeam counterpart.

2.2.2. Doppler measurements. Another example of the value of parametric directivity is afforded by application of the same apparatus to Doppler detection. Since most everything of interest in the ocean is in movement, we are obliged to understand the dynamics of the process. With respect to the medium, this involves relating the directional spectra of scatterers in motion to the directional properties and motion of the sonar in order to arrive at the Doppler spectra it will observe. Although this process is intuitively understood, it is by no means delineated, and important work along these lines is in progress (8).

Conceptually, backscattered Doppler received at some angle θ on a sonar beam can be modeled by

$$\Delta f = 2(f_o/c_o)(\vec{v}_s - \vec{v}_m) \cdot D(\theta)\vec{e}_\theta \quad , \tag{6}$$

where f_o is the carrier frequency, c_o is the sound speed, $\vec{v}_s$ is the velocity vector of the ship carrying the sonar, $\vec{v}_m$ is the velocity vector of the segment of the medium in view (which may contain a target), $D(\theta)$ is the directivity function of the sonar, and $\vec{e}$ is the unit vector of the angular position on the beam relative to that of the ship's path. This simplified result would give the spectrum of backscattered Doppler, if all of the

scatterers in the medium had the same target strength. Actually, $\vec{v}_m$ is itself a spectrum that can be quite complicated for the case of a turbulent medium. Since each inhomogeneity there has its own cross section as well as velocity, rigorous solutions of the problem are usually expressed in terms of a scattering integral.

Eq. (6) nonetheless illustrates an important aspect of Doppler measurements that involves the influence of the directivity function $D(\theta)$. This function weights Doppler frequency measurements in reverberant environments such that the broader the beam the broader the Doppler spectrum received. In this case, precise Doppler data can only be acquired with systems that have good directivity.

Some experimental results on this topic are depicted in Fig. 5. A spherical target was towed at mid depth toward a fixed soundhead operating at 20 kHz in the aforementioned lagoon experiment. The target was moving at approximately 2 kt. The surface of the water was driven by the wind at a comparable velocity along the same direction of motion. A 50 msec cw pulse at 15 kHz was used to insonify the target for Doppler measurements. In processing, the received signal was beat against the transmit signal, and the Doppler shifted frequencies were obtained at baseband by low pass filtering. These are displayed in the figure in quasi-3D plots that show the range dependence of Doppler signal amplitude (on the vertical axis) for successive pings (time history) as the target closes range.

It can be seen that the target appears clearly in the narrowbeam data. Its Doppler frequency is also measurable from the baseband oscillations along the range, or equivalently, the instantaneous time axis. The broadbeam system views more of the

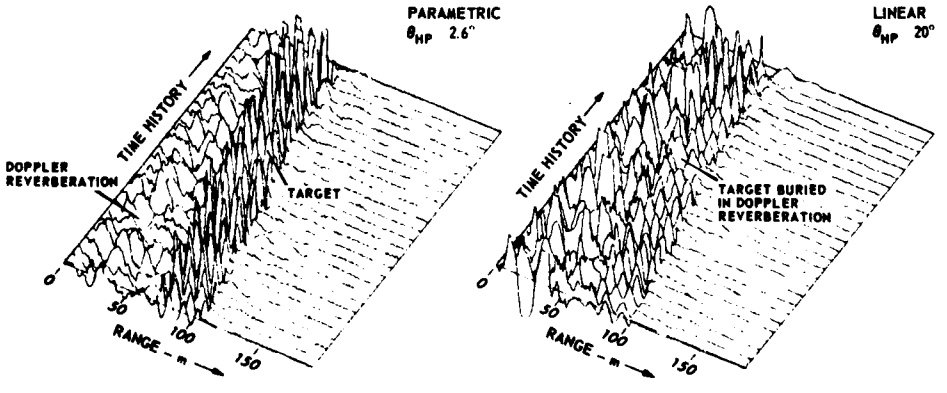

Figure 5. Doppler data from a moving target masked by moving surface reverberation.

moving surface and therefore experiences more Doppler noise which masks the target and makes detection and measurement more difficult.

2.3. Directivity of Harmonic Radiations

Another important directivity aspect of nonlinear acoustics lies in the area of harmonic radiations created in the nonlinear distortion and shock formation process. As is well known, the velocity varies within a high intensity waveform in proportion to the local particle velocity. This causes a steepening of the waveform in the time domain, which is equivalent to the creation of harmonic components in the frequency domain.

The harmonics are attractive because of their great directivity. It has been shown (9) that the directivity function of the nth harmonic is equal to that of the fundamental raised to the nth power, or

$$D_n(\theta) = D_1^n(\theta) \quad . \tag{7}$$

Thus, as one progresses to the higher harmonics, the width of the beam decreases and the minor lobe suppression increases. These are desirable features in imaging applications.

The amplitudes of the harmonic radiations can be quite high. At initial shock formation, the 2nd, 3rd, and 4th harmonics are only 8, 12, and 15 dB, respectively, below the fundamental. In hard shock, their amplitudes go as the reciprocal harmonic number, so that the same respective harmonic amplitudes will be 6, 10, and 12 dB below the fundamental (9).

2.4. Applications of Directive Harmonics

We have conducted several experiments with harmonic sonar using a rectangular transducer measuring 1.0 x 0.1 m. It was energized at a fundamental frequency of 100 kHz in 200 μsec cw pulses with 1.3 kW of pulse power. With a transducer efficiency of 50%, this yields a source intensity of 0.7 W/cm^2. Since the beam is only 0.8° x 8° in half-power width, it has a high directivity and source level, which means that harmonic radiations are created as the high intensity pulse propagates through the water. Echoes from targets are received by a wideband hydrophone, amplified, and passed through any of a series of narrow bandpass filters tuned to the harmonic frequencies. The harmonic signals are processed and displayed in a range/bearing (B scan) format.

2.4.1. Detection sonar. A typical illustration of some of the advantages of harmonic echo scanning is shown in Fig. 6. A point target at a range of 100 m is depicted with both the

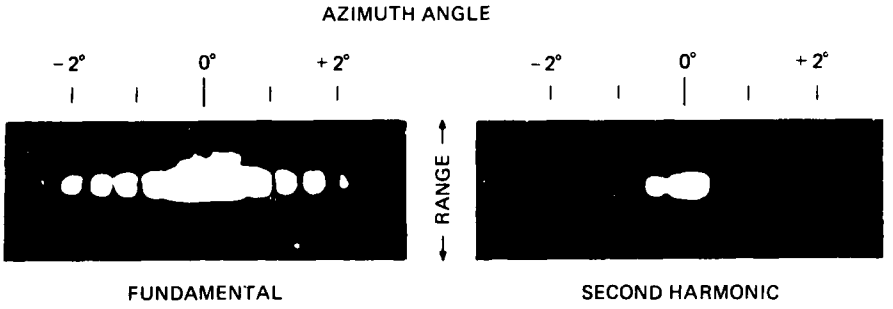

Figure 6. Comparison of point target detection performance.

fundamental and its second harmonic component. The fundamental radiation has a half-power resolution of 0.8° or 1.4 m in bearing and 0.3 m in range, with a minor lobe suppression of 13 dB. A scan taken at the fundamental frequency shows the target in a condition of display saturation, which is a quite common occurrence in sonar displays. The second harmonic data demonstrate the alleviation of these undesirable effects, even though the video gain was normalized to the same peak input voltage. With the second harmonic, the half-power beamwidth was reduced to 0.5°, yielding a resolution cell 0.9 m in azimuth by 0.3 m in range. Also, the minor lobe suppression was increased to around 20 dB (it should have been 26 dB). The target display is much more compatible with the sonar's resolution capability and the adjustment of the display is much less critical.

2.4.2 Imaging Sonar. Further demonstration of the dynamics of harmonic echo scanning is afforded by the data of Fig. 7 which depicts the viewing of larger targets. Here the beam patterns are shown at left for the 1st through 5th harmonics of the experiment at hand. Range/bearing images of a cylinder are shown at right, with each display corresponding to a particular harmonic echo scan, each made at a range of 100 m. With the fundamental radiation, the beam is almost as large as the target. As a result, one really sees only some large "blobs", probably due to echoes from each end of the target. Reception of these echoes with the minor lobes is also evident. The sidelobe echoes are not a problem in the second harmonic data. With the third harmonic, the orientation of the target becomes clearly evident. Data for the fourth harmonic shows a fair representation of the size of the target. This trend continues to the fifth harmonic, although the display has become somewhat sparse, perhaps for nonacoustic reasons.

The data displayed in the center column of Fig. 7 are for the viewing of an object much larger than the original beam.

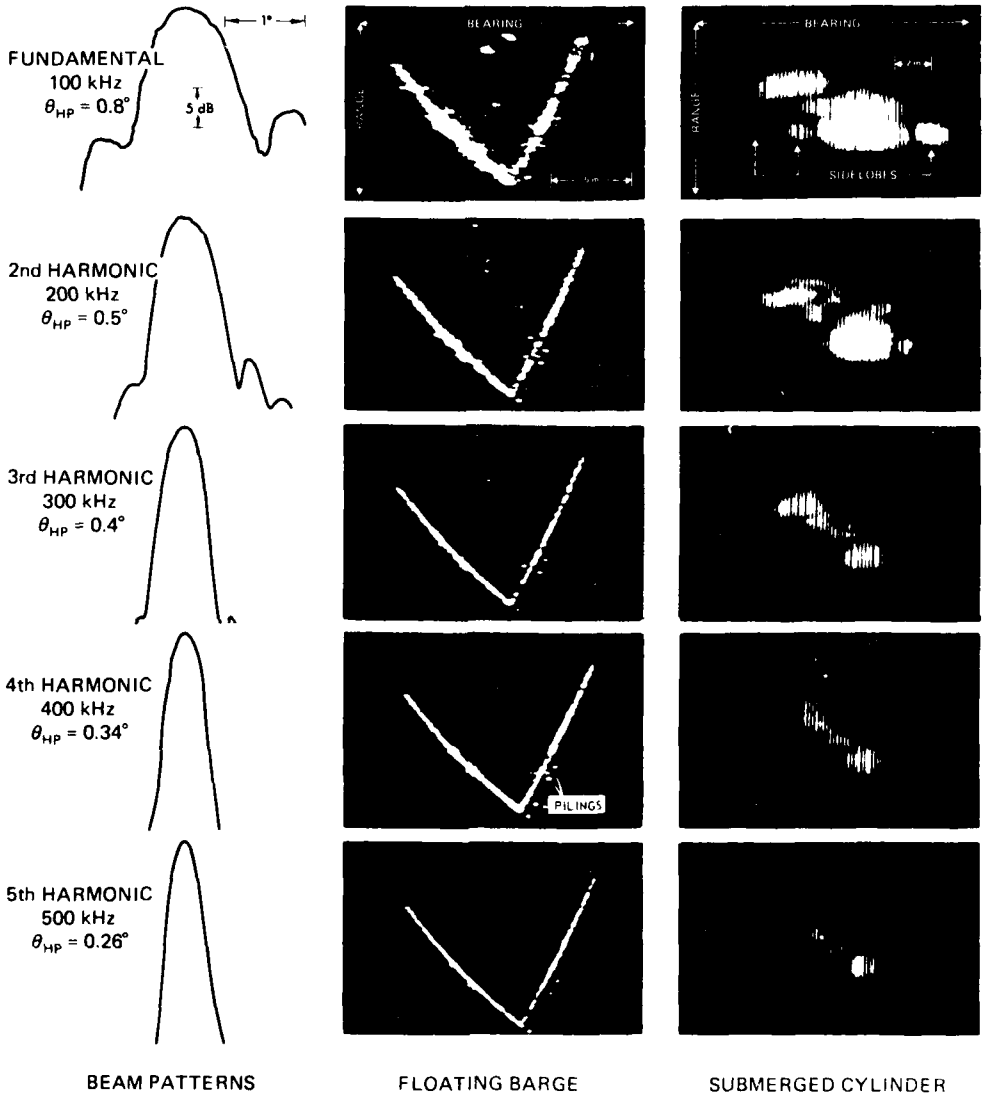

Figure 7. Imaging with the harmonic radiations.

These are range/bearing scans of a barge having a diving platform with pilings attached. As can be seen, the definition in the field of view becomes progressively better with increase in harmonic number, angular resolution, and minor lobe suppression. At about the fourth harmonic, the four pilings (15 cm in diameter) becomes clearly evident.

Although it can be argued that the harmonic radiations are subject to more absorption than the fundamental, it is nonetheless

true that many applications are not precluded by absorption limited effects. It appears reasonable, for example, to acquire crude images with the low frequency fundamental for initial study and then develop sharper images with the harmonics, as the range-dependent absorption factor permits.

2.5. Bandwidth of Parametric Sources

The frequency response of a parametric array may be obtained from the principle of superposition applied to any of the steady state solutions for difference frequency sound. This has been formulated (10) for the Westervelt solution (6) on the acoustic axis as

$$p_s(\omega_s) \propto \omega_s^2 \int_{-\infty}^{\infty} p_1(\omega)\ p_2(\omega+\omega_s)d\omega \quad , \tag{8}$$

where ω_s is the difference frequency and $p_1(\cdot)$ and $p_2(\cdot)$ are the two primary (interacting) pressures. This result is equivalent to a crosscorrelation integral in product with the difference frequency squared. It is a very straightforward and powerful result that has been used with the theorems of convolution, Fourier transform, etc., to obtain the transient response of the parametric array (10).

This result can also be used to determine the difference frequency response of a given system by considering the frequency response of the primary radiations in their own operating band. Primary projectors are almost invariably tuned devices that are impedance matched to their power amplifiers at their resonance frequencies. Each projector has a limited Fourier spectrum over which it can transmit sound at high intensity. Consideration of the steady state frequency response enables Eq. (8) to be reduced to

$$\frac{dp_s(\omega_s)}{d\omega} \propto \omega_s^2\ p_1(\omega_1)\ p_2(\omega_2) \quad , \tag{9}$$

where $\omega_s=\omega_1-\omega_2$, and ω_1, ω_2 denote the primary frequencies utilized. To treat a practical example, let us suppose that we have a typical projector in the primary frequency band whose half-power bandwidth, $\Delta\omega_{HP}$, is about 15% of the resonance frequency, ω_o, and whose response is a Gaussian function of frequency, i.e.,

$$p = p_o\left[\exp -a^2(\omega-\omega_o)^2\right] \quad , \tag{10}$$

where a = 7.85 sec/rad, a constant. A projector of this type would have a $Q=\omega_o/\Delta\omega_{HP}$ of 6.7. This function is plotted at left

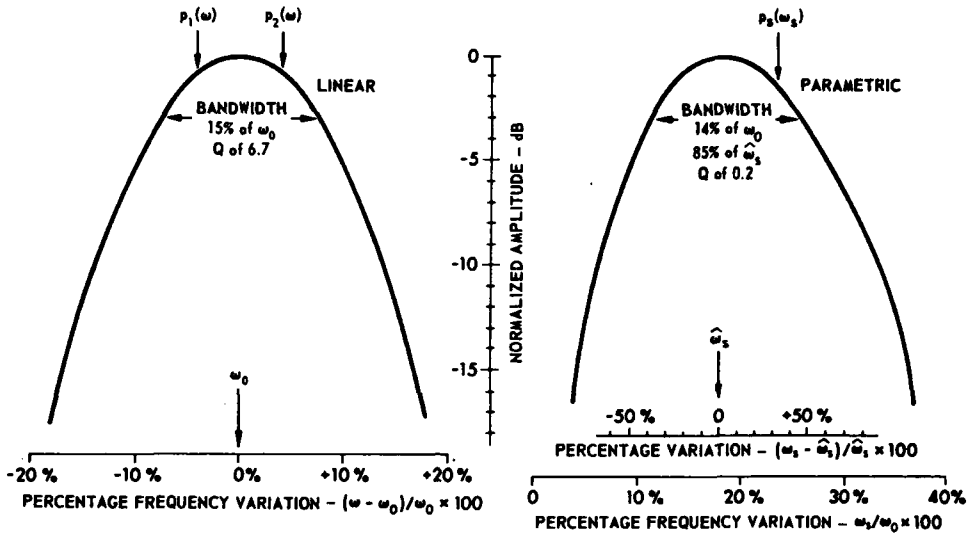

Figure 8. Parametric bandwidth and frequency response characteristics for a typical primary source.

in Fig. 8. We further assume that the two primary radiations are driven symmetrically about the resonance frequency ω_o, as shown.

Application of Eq. (9) to the difference frequency response yields the plot at right in Fig. 8. It can be seen that the difference frequency pressure maximizes at $\hat{\omega}_s \approx 18\%$ of the primary frequency. There is essentially a bandwidth translation from primary to difference frequency sound, as shown. In terms of $\hat{\omega}_s$, the difference frequency radiation would be capable of about an 85% bandwidth, or a Q of 0.2. These features, as well as the asymmetric shape of the difference frequency spectrum, are a result of the dependence of Eq. (8) on the $p_1(\cdot)\ p_2(\cdot)$ product, upward weighted by multiplication with ω_s^2. As a result, the difference frequency is capable of a -3 dB bandwidth greater than one octave, and is useful over even larger bandwidths.

2.6. Processing of Wideband Parametric Signals

Given that a parametric sonar will usually have greater directivity and bandwidth than a comparable linear device, it is worthwhile to consider the difference this may make in signal processing. These attributes may be utilized in various ways, from measuring the frequency response of a resonant target in a reverberant environment, to extracting a weak signal from noise or reverberation with wideband processing, etc. Since it is not our purpose here to invent new active sonar processing techniques,

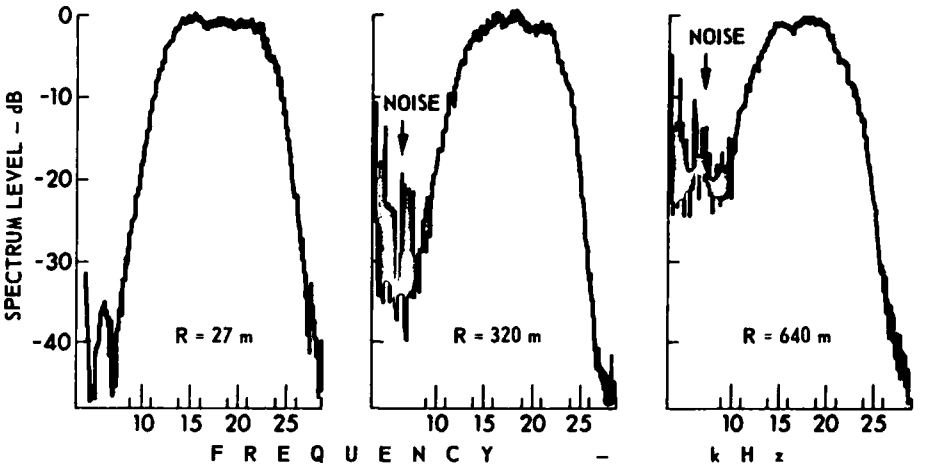

Figure 9. Spectra of a wideband FM chirp at several ranges in a shallow water waveguide.

we will restrict the discussion to existing, well-known procedures.

2.6.1. Spectral measurements. The bandwidth capability of a parametric array may be used to obtain the frequency response of a wide variety of resonant structures as well as the spectral response of environmental features (reverberation, model propagation, etc.). The FM chirp signal is especially suited to rapid, and practically instantaneous, acquisition of this type of data.

An example is afforded by the results of Fig. 9, which shows some normalized propagation spectra associated with the transmission of a wideband parametric pulse in the previously described lagoon experiment. Here the source and receiver were at mid depth in the 1.4 m waveguide and the signal was swept over a little more than an octave in an FM chirp 3.5 msec long. The wind driven surface waves during the acquisition of data had a standard deviation $2\sigma = 6.2$ cm. Spectra measured with an analyzer bandwidth of 1 Hz are shown at three ranges. At 27 m, the spectrum has a half-power width of 21 kHz, but it falls to 18.5 kHz at 320 m and 16 kHz at 640 m, which translates into a loss in bandwidth of 8.2 Hz per meter of propagation range. Jensen and Kuperman (11) have suggested that the rounding off of the spectrum at the lower frequencies is due to bottom loss, while losses at the upper edge of the spectrum may be due to volume and surface scatterers. The capacity of the medium to sustain wide bandwidth signals is an important issue in underwater acoustics. It is interesting and useful to study the governing mechanisms with different research tools.

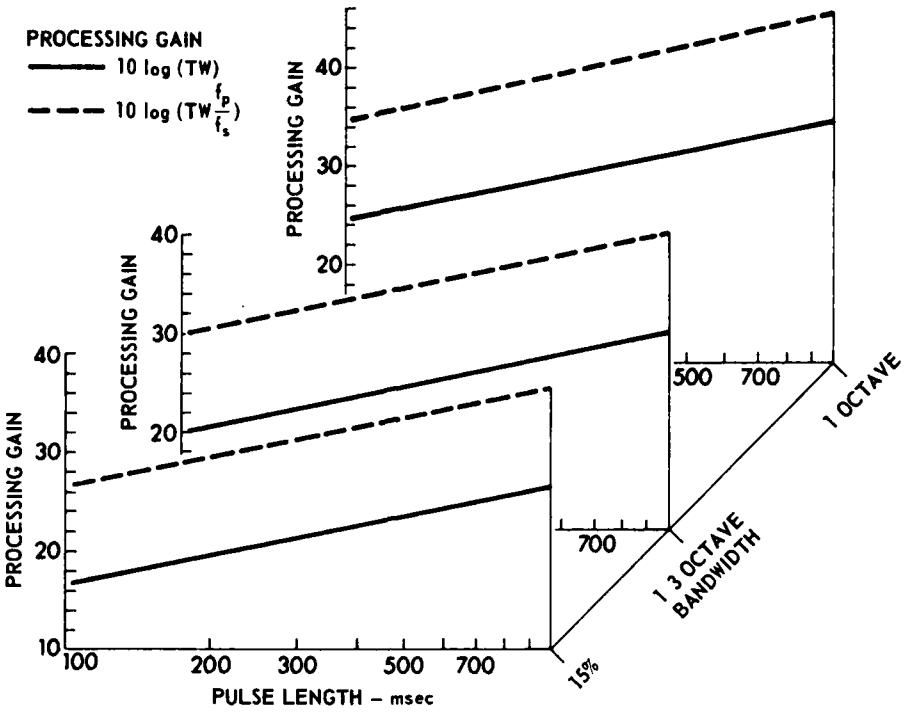

Figure 10. Implications for processing gain as a function of attainable time-bandwidth properties.

2.6.2. Large time-bandwidth processing. For the simple processors in common use, one can talk in terms of coherent or incoherent techniques. The latter, in the form of linear or square law detector/averager systems, may be preferred for distributed targets or where the medium multipath destroys the coherence of the signal. The former, in the form of matched filter systems (replica correlator, delay line, or other implementation) may be preferred when the degradation of signal coherence is not prohibitive. Both approaches have in common the fact that the processing gain is proportional to the time-bandwidth product, TW, of the signal.

To illustrate the capability of parametric arrays in this regard, we assume a coherent processor whose processing gain against white Gaussian noise is (12)

$$\text{P.G.} = 10 \log TW \quad . \tag{11}$$

Some results for an assumed center frequency of 3 kHz are shown in Fig. 10 as a function of pinglength for 15%, 1/3 octave, and 1 octave bandwidths. There is a 3.5 dB improvement in going from

15% bandwidth to 1/3 octave, and an 8.2 dB improvement in going to a 1 octave bandwidth. Whether or not the medium or the target can accommodate large bandwidths is an issue worthy of resolving. If such large bandwidths are attainable, they will probably occur at low frequencies, where propagation losses are minimized and where low ka target strengths can be realized. Here, the targets would behave more like point targets with fairly omnidirectional scattering patterns. Although it is difficult to realize low ka systems, those with ka=1-3 appear attractive. The parametric array approach to low ka systems utilizes nonlinear acoustics' strongest attribute--low frequencies with small transducers.

If the noise is reverberation, there is an added signal-to-noise gain that is equivalent to a processing gain. This can easily be included in Eq. (11) if we recognize that at low audio frequencies, the beamwidth of the parametric array will be dominated by the product directivity of the primaries, D_p, in the convolution of Eq. (2). The difference frequency beamwidth will then be slightly larger than the product pattern beamwidth. For surface reverberation, the processing gain improvement in going from a conventional linear system to a parametric system (of the same size operating at the same frequency) is proportional to the ratio of their respective insonified areas. This is

$$P.G_{REVERB} = 10 \log\left(\frac{S_{o\text{-}LIN}}{S_{o\text{-}PAR}}\right) = 10 \log\left(\frac{\theta_{HP\text{-}LIN}}{\theta_{HP\text{-}PAR}}\right) \sim \frac{f_p}{f_s} \qquad (12)$$

where the downshift ratio f_p/f_s is again the ratio of primary to difference frequencies. The dashed lines in Fig. 10 represent the relative merit of parametric directivity for this case.

Directivity, of course, is as useful as bandwidth for processing gain in a reverberant situation and it may be easier to achieve and maintain. More importantly, it may often be the essential factor that precludes all other considerations. As Laval points out (13), the detection of a signal in reverberation is either a "go" or "no go" situation. One simply has to have enough suppression to recognize the target in the first place, irrespective of the source level or efficiency.

3. NONLINEAR RECEIVERS

The same general principles at work in generation of low frequency signals by nonlinear sources are involved in reception of low frequency acoustic waves by a nonlinear receiver. In the parametric source, information in the two high frequency primary waves is translated by intermodulation to a lower frequency region because of the inherent nonlinearity of the pressure density

relationship of water. On the other hand, in the nonlinear receiver the information in a low frequency signal wave is translated to the sidebands of the pump wave by intermodulation of the low frequency signal wave and the pump wave.

In the parametric source, essentially all of the signal processing is performed by the water since differential absorption removes the high frequency primary waves and leaves only the low frequency signal that propagates to long ranges. However, in the case of the nonlinear receiver, the desired information exists as low level modulation sidebands of the pump signal, which places severe constraints on the signal processing used to recover the information. Signal processing techniques are the focus of the remainder of this paper, but to introduce that topic, some background material about the nonlinear receiver will be given first to establish a common base of terminology.

3.1. Background

The nonlinear acoustic receiving array, or parametric receiver, uses the inherent nonlinearity of the water to achieve directional reception of low frequency acoustic waves with only two small high frequency transducers and some associated electronic hardware. This concept was first suggested by Westervelt, almost as an afterthought, in his classic paper on parametric acoustic arrays (6). In the next few years, a number of theoretical and experimental investigations followed, most of which emphasized demonstrating existence of the phenomenon and developing and validating mathematical models to describe the basic physics of the process, e.g., Truchard (14).

The basic elements of the parametric receiver are the pump oscillator and power amplifier, two high frequency transducers, and the receiving electronics. The pump oscillator and power amplifier generate a stable, continuous, high frequency signal and amplify it to a level sufficient to produce the desired pump acoustic level in the water. The pump signal is projected from one of the transducers (pump) and received by the second transducer (hydrophone) located a distance L from the pump. Ambient low frequency acoustic waves propagating through the same water volume will interact nonlinearly with the pump wave to generate intermodulation products. The function of the receiver electronic hardware is to recover the information contained in the ambient signals by demodulating the interaction products which appear as modulation sidebands on the pump carrier. Thus an ambient acoustic wave of frequency f_s produces an electrical signal at the output of the receiver electronics which is also of frequency f_s.

Zverev and Kalachev (15) expressed the pump signal and the intermodulation products at the hydrophone in closed form as a

phase modulation of the pump wave by the ambient acoustic waves. If the pump wave is an ideal sinusoid $\cos(\omega_o t)$, the signal at the hydrophone can be represented as

$$s(t) = \cos(\omega_o t + \phi_a(t) + \psi) \quad , \tag{13}$$

where $\phi_a(t)$ is a phase modulation due to the nonlinearity of the water and ψ is a phase shift related to the propagation delay from the pump to the hydrophone. The acoustic phase modulation term is given by

$$\phi_a(t) = \frac{[\beta - (1-\cos\theta)]\ \omega_o\ P_s}{\rho_o c_o^3} \frac{\sin[(k_s L/2)(1-\cos\theta)]}{(k_s L/2)(1-\cos\theta)} \quad . \tag{14}$$

In this expression θ is the plane angle measured from the line joining the pump and hydrophone, P_s and k_s are the amplitude and wave number, respectively, of the signal to be detected, L is the pump-hydrophone separation, ω_o is the pump frequency, ρ_o and c_o are the equilibrium density and sound speed, respectively, and $\beta(=1+B/2A)$ is the coefficient of nonlinearity of the medium (approximately equal to 3.5 in seawater).

The directional response of the parametric receiver can be obtained from Eq. (14) and is given by

$$D(\theta) = \frac{\beta - (1-\cos\theta)}{\beta} \frac{\sin[(k_s L/2)(1-\cos\theta)]}{(k_s L/2)(1-\cos\theta)} \quad . \tag{15}$$

From Eq. (15) it is clear that the directional response of the parametric receiver is symmetric about the maximum response axis which is in the direction of a line extending from the hydrophone through the pump. Furthermore, the directional response is independent of the pump frequency; it depends only upon the pump-hydrophone separation and the wavelength of the signal to be detected. Although the array synthesized in the interaction volume is actually a volumetric array, the directivity characteristics of the synthesized array are similar to those of a continuous, end-fire array of length L. Thus, the half-power beamwidth is given in radians approximately by

$$\theta_{HP} = 1.9\sqrt{\lambda_s/L} \quad , \tag{16}$$

where λ_s is the acoustic wavelength of the signal to be detected. It is the end-fire array effect that provides the directivity of the parametric receiver and hence its ability to discriminate against the low frequency ambient noise that may otherwise mask the signal wave.

The detection of low frequency signals in the ocean is closely related to the ability of the acoustic sensor to discriminate against low frequency ambient noise and thereby improve the signal-to-noise ratio (S/N) compared to a simple, omnidirectional sensor. One measure of the S/N improvement of an acoustic sensor is spatial processing gain (SPG), which is the ratio of the noise received by an omnidirectional sensor to the noise received by the directional acoustic sensor. If the noise field is isotropic, the SPG is equal to the directivity index (DI) of the sensor. For large acoustic apertures the DI of the parametric receiver asymptotically approaches the DI of a continuous end-fire array of the same acoustic aperture,

$$DI = 10 \log(4L/\lambda_s) \quad . \tag{17}$$

Although the ambient noise field is rarely isotropic, the DI is a convenient and useful measure for first order comparisons of different acoustic sensors.

Since the ambient noise field is usually anisotropic, the response of the sensor to noise from the back side is very important. For $L/\lambda_s >> 1$, the ratio of the maximum response of the parametric receiver to the envelope of the back lobes is given in decibels by

$$F/B = 20 \log(14\pi L/3\lambda_s) \quad . \tag{18}$$

Both the DI and the F/B of the parametric receiver are functions of the acoustic aperture and are independent of the pump frequency.

Any acoustic sensor will have some self-noise floor which represents the noise pressure equivalent to the internal, or self-noise, sources. Clearly, the self-noise of a sensor must be less than the amplitude of the signal to be received by the sensor. The self-noise contributors in the parametric receiver must be identified and controlled if a S/N improvement commensurate with the directivity characteristics is to be achieved. The principal noise sources in the parametric receiver have been identified and selection of parameter values to minimize the effects of these noise sources have been discussed previously (16-19).

The difficulty, and the importance, of the receiver electronics design can be appreciated from the following. Since the water is only weakly nonlinear, the interaction components (modulation sidebands) are very low level signals. For spherically spreading pump waves, Berktay and Shooter (20) derive an expression for the axial value of the interaction component pressure amplitude as

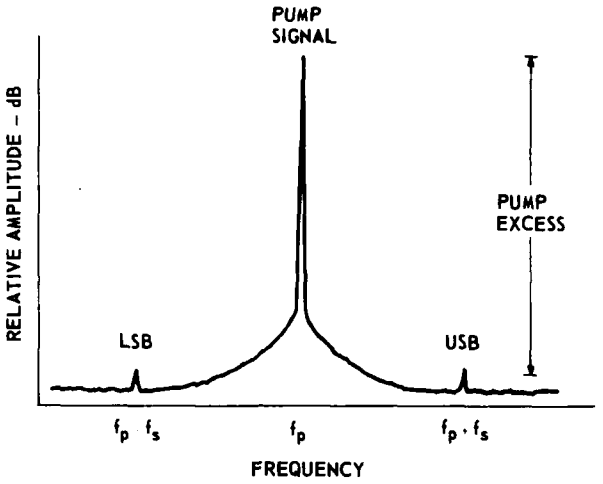

Figure 11. Near-sideband signal spectrum of the parametric receiver showing the upper and lower sideband signals.

$$p(L) = \frac{\omega_o \beta P_o P_s}{2\rho_o c_o^3} \exp(-\alpha_o L) \quad , \tag{19}$$

where P_o is the pressure amplitude of the pump wave at unit distance from the pump, α_o is the absorption coefficient at the pump frequency ω_o, and we have made use of the fact that $\omega_o >> \omega_s$ to simplify the expression.

Berktay and Muir (21) define pump excess as the ratio of the amplitude of the pump signal to the amplitude of the interaction component, measured at the hydrophone. This is illustrated in Fig. 11 which shows a hypothetical spectrum at the output of the hydrophone when the parametric receiver is receiving an acoustic wave of frequency f_s. The large amplitude component at frequency f_p represents the pump signal. The interaction components denoted "USB" and "LSB" represent the upper and lower sidebands resulting from modulation of the pump wave by the acoustic wave of frequency f_s. For cases of practical interest, the amplitude of the interaction components will be comparable to the low frequency ambient noise within the parametric receiver beam. Under these conditions, the pump excess of a parametric receiver for passive sonar application to receive low audio frequencies in the ocean will be in the 140 to 170 dB range. Thus, although the nonlinear acoustic process is phase modulation, we can ignore the higher order sideband components, approximate the process as a linear modulation, and use linear modulation techniques to recover

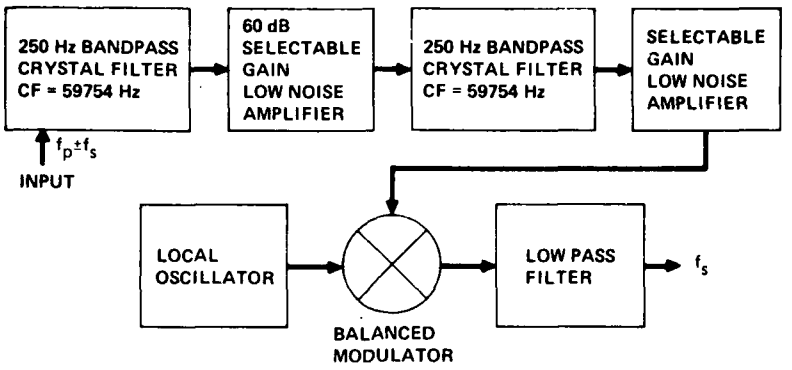

Figure 12. Block diagram of the bandpass receiver.

the sideband signals. The modulation index is then equivalent to the reciprocal of the pump excess, and it is clear that a receiver capable of recovering sideband signals with modulation indices in the range of 10^{-7} to 3×10^{-9} will be required.

3.2. Sideband Recovery Techniques

Three techniques have been used that satisfy some or all of the requirements of the processor in various parametric receiver configurations. The common element in each of these techniques is their dependence upon the resonance properties of quartz crystals. In two of the methods, crystal bandpass or crystal band elimination (notch) filters are used to suppress or reject the high amplitude pump frequency component (carrier) while simultaneously passing the modulation sidebands. In the third technique, the modulation sidebands are recovered by mixing the parametric receiver signal with a reference signal from a crystal stabilized, phase locked loop oscillator in a high performance diode mixer. Each of these techniques has advantages and disadvantages that will be discussed in the following.

3.2.1. Bandpass receiver. It is well known that the information in a modulated carrier is redundantly represented in the two sidebands. Single sideband (SSB) communication systems have used this fact to advantage for many years. Thus in the case of the parametric receiver, it is sufficient to recover only one sideband signal. One method of accomplishing this is to use a SSB crystal filter to reject the carrier and one sideband while passing the other sideband. Another method is to use bandpass crystal filters that pass only that portion of one sideband that is of interest.

The latter technique was used in early experiments to investigate the self-noise sources in the parametric receiver (17). A block diagram of the receiver used in those experiments is shown in Fig. 12. The skirts of the cascaded 250 Hz bandpass crystal filters suppressed the high level carrier and the low noise amplifiers provided buffering and sufficient amplification of the bandpassed SSB signal to drive a balanced modulator. The demodulated signal was low pass filtered to yield the baseband signal. This receiver had a 5 dB noise figure at an input impedance of 10 kΩ and was used with a 60 kHz crystal controlled pump signal to receive acoustic signals over the 125 to 375 Hz frequency range.

The bandpass receiver is relatively simple and easy to implement because low noise integrated circuit preamplifiers and wideband balanced modulators are readily available. A minimum of electronic circuitry is required to translate the SSB signal to baseband. The bandpass receiver is useful for some experimentation and perhaps for limited applications; however, it has several significant disadvantages.

One disadvantage of the bandpass receiver technique is that the shape factor of SSB or bandpass crystal filters limits the carrier suppression that can be obtained when the passband extends to within a few hertz of the carrier frequency. This limits the low frequency response of the receiver and, hence, the parametric receiver. Another disadvantage is the maximum carrier-to-spectrum sideband noise ratio (C/SN) that can be achieved. In the bandpass receiver described previously, the maximum C/SN observed during experiments was 152 dB. The bandpass receiver was also very sensitive to vibration induced spurious noise at high carrier levels.

3.2.2. Band elimination receiver. Band elimination crystal filters were first used for carrier suppression in parametric receiver experiments by Barnard et al. (22). The amplitudes of high level pulsed sinusoids used in these experiments were detected to plot beam patterns or to compare with predicted interaction component amplitudes. The sidebands were not demodulated to yield a broadband receiver and signal frequencies below 1000 Hz were not investigated.

The band elimination filter approach was combined with concepts from the bandpass receiver in developing a band elimination receiver capable of detecting sideband signals over the 35 to 4000 Hz frequency range at carrier-to-sideband ratios approaching 180 dB. Figure 13 shows a block diagram of that receiver, which performs the basic functions of carrier suppression, sideband signal amplification, frequency translation, and sideband separation. The band elimination receiver is functionally similar to the bandpass receiver described previously but the change to

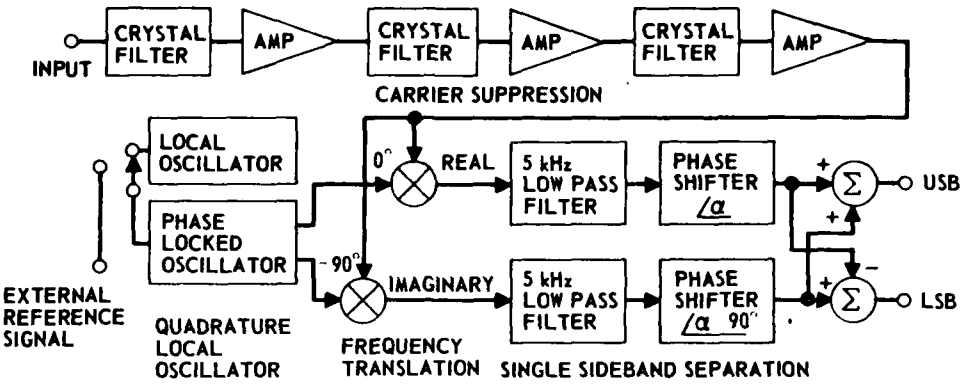

Figure 13. Block diagram of the band elimination receiver.

band elimination filters required a more complex demodulation process to accommodate the double sideband (DSB) signal.

Carrier suppression and sideband amplification are provided by cascaded crystal filters and low noise amplifiers. Each filter provides greater than 40 dB of attenuation at frequencies less than 10 Hz from the 65 kHz carrier frequency while signals with frequencies greater than 35 Hz from the carrier frequency are attenuated less than 3 dB. Insertion loss of each crystal filter is less than 2 dB over the passband. The low noise amplifier provides amplification with less than 1 dB of additive noise to the signal from the crystal filter terminated by a 15 kΩ resistor. This combination gives a receiver noise figure of 5 dB for the 15 kΩ input impedance of the receiver.

The cascaded crystal filters attenuate the carrier by greater than 140 dB to yield a double sideband suppressed carrier signal at the output of the last crystal filter. To separate the sideband signals, this suppressed carrier signal is amplified and coupled into a pair of balanced modulators operating in phase quadrature. The signals from the modulators are low pass filtered to remove the higher order product frequencies and any residual carrier. The low passed signals are phase shifted by a broadband quadrature phase shift of 90° between the two signal channels. The signals from the phase shift networks are combined with appropriate polarities to yield the upper and lower sideband signals simultaneously.

A phase locked loop (PLL) oscillator generates the carrier frequency quadrature reference signals for the balanced modulators. The PLL oscillator contains a digital divider network and a voltage controlled oscillator operating at four times the carrier frequency. The final stages of the divider network are driven with complementary waveforms to produce the carrier frequency quadrature

reference signals. The carrier frequency reference signal for the PLL oscillator is normally supplied by an internal crystal stabilized local oscillator; however, a switch selectable input allows an optional external reference signal to be used if needed.

The equivalent input noise of the band elimination receiver was measured at -151 dB re 1 V/$\sqrt{\text{Hz}}$ over the 35 to 4000 Hz frequency range. Maximum power dissipation in the crystal filter is 1 mW, which corresponds to a maximum carrier level of 29 dB re 1 V from a 15 kΩ source. Thus the receiver should be able to detect signals 180 dB below the maximum carrier level. During development and testing of a 340 m parametric receiver at Lake Travis (Texas) signals as small as -168 dB referenced to the carrier level were received and displayed (23). Rohde et al. describe this receiver in greater detail and give test results from the development (24).

The band elimination receiver discussed in this section is a very effective processor and it satisfies the requirements of the parametric receiver under a variety of conditions. It is capable of detecting signals with smaller modulation indices than any other currently available receiver. The simultaneous availability of both sideband signals is especially useful in some investigations (25). The most serious disadvantages of this receiver are the high input impedance of the crystal filters and sensitivity of these filters to spurious noise induced by vibration of the filters at high carrier levels. The linear characteristics of the band elimination receiver can be a disadvantage in applications where the transducers are subjected to large amplitude vibrations. This effect and a technique for reducing the detrimental effects of transducer vibration are discussed in the next section.

3.2.3. Phase locked loop receiver. Because the water is only weakly nonlinear, in virtually all cases of practical interest the acoustic phase modulation index, $\phi_a(t)$, is very small and Eq. (13) can be simplified to

$$s(t) = \cos(\omega_o t+\psi) - \phi_a(t) \sin(\omega_o t+\psi) \quad . \tag{20}$$

Reeves et al. (26) have extended the analysis to include transducer vibration. If the pump and hydrophone are not stationary relative to each other, the phase shift ψ is not a constant but is given by

$$\psi(t) = \psi_o + \phi_m(t) \quad , \tag{21}$$

where ψ_o is the phase shift due to propagation delay between the mean positions of the pump and hydrophone, and $\phi_m(t)$ is the phase variation caused by displacements of the transducers from their mean positions. In contrast to $|\phi_a(t)|$, which is small in almost

all cases of interest, $|\phi_m(t)|$ may or may not be small in many applications, depending upon the vibration amplitudes.

If $|\phi_m(t)| \ll 1$, Eq. (13) can be simplified as previously to yield

$$s(t) = \cos(\omega_o t+\psi_o) - [\phi_a(t)+\phi_m(t)] \sin(\omega_o t+\psi_o) \quad . \quad (22)$$

In this case the modulating signal is the sum of the acoustic modulation due to nonlinearity of the water and the vibration modulation due to transducer motion. Under these conditions a linear receiver such as the band elimination receiver is adequate.

On the other hand, if $|\phi_m(t)|$ is not small relative to a radian, Eq. (13) can only be linearized in $\phi_a(t)$, which gives

$$s(t) = \cos(\omega_o t+\phi_m(t)+\psi_o) - \phi_a(t) \sin(\omega_o t+\phi_m(t)+\psi_o) \quad . \quad (23)$$

Reeves et al. (26) have shown that large amplitude transducer vibration, which produces a convolution of the vibration modulated carrier spectrum with the acoustic spectrum as shown by Eq. (23), causes distortion of the acoustic signal when received by a linear receiver such as the band elimination receiver. A phase locked loop technique was suggested as a possible solution to this problem.

Investigation of the phase locked loop receiver technique has been continued by Lamb (27). He has analyzed the carrier tracking phase locked loop and designed a PLL demodulator for use with the parametric receiver. A block diagram of this PLL receiver is shown in Fig. 14. The PLL receiver operates as a closed loop servo system with signal phase as the controlled variable. The signal from the hydrophone is impedance transformed and coupled into the double balanced diode mixer which has a very large dynamic range. The output of the mixer is amplified and low pass filtered to provide the control voltage for the low noise voltage controlled oscillator, which in turn provides the carrier frequency reference signal for the mixer. The accuracy

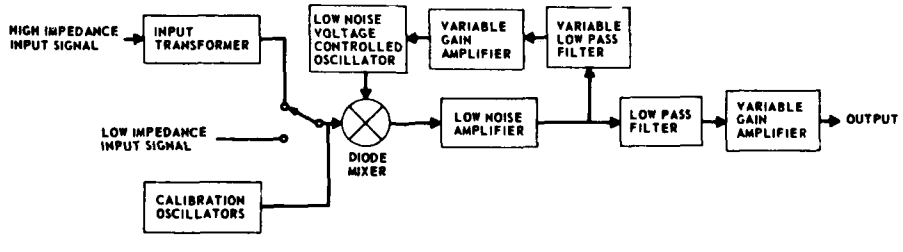

Figure 14. Block diagram of the phase locked loop receiver.

with which the voltage controlled oscillator tracks the phase variations of the input signal is a function of the loop gain and the variable low pass filter allows the loop bandwidth to be changed easily. Tests with a crystal stabilized low noise oscillator showed that the PLL receiver noise floor was -160 dB referenced to the carrier level.

The performance of the PLL receiver was compared to that of the band elimination receiver in processing the output of a parametric receiver hydrophone undergoing large amplitude, low frequency vibration. The output of the band elimination receiver is shown in Fig. 15(a). A 70 Hz acoustic signal was being received while the parametric receiver hydrophone was mechanically vibrated at a frequency of 0.53 Hz with a peak displacement of 4 mm. The vibration induced modulation sidebands about the 70 Hz signal are clearly evident. The output of the PLL receiver processing the signal from the parametric receiver under the same conditions is shown in Fig. 15(b). The improvement in the intermodulation sidebands is approximately 20 dB for these data which were obtained with a 10 Hz loop filter. Greater reductions of the intermodulation sidebands were obtained with a narrower loop filter. Clearly under these conditions, detection of narrowband signals would be more easily accomplished with the PLL receiver.

The major disadvantage of the PLL receiver at this time is the maximum carrier-to-sideband ratio of 160 dB. An improvement of 10 to 20 dB in this parameter is needed for some applications.

ACKNOWLEDGMENTS

The authors wish to thank L. M. Deuser for his assistance in analysis and reduction of data from the shallow water lagoon experiments, and L. L. Mellenbruch who conducted many of the imaging experiments. This work was supported by the US Navy Office of Naval Research and the Defense Advanced Research Projects Agency.

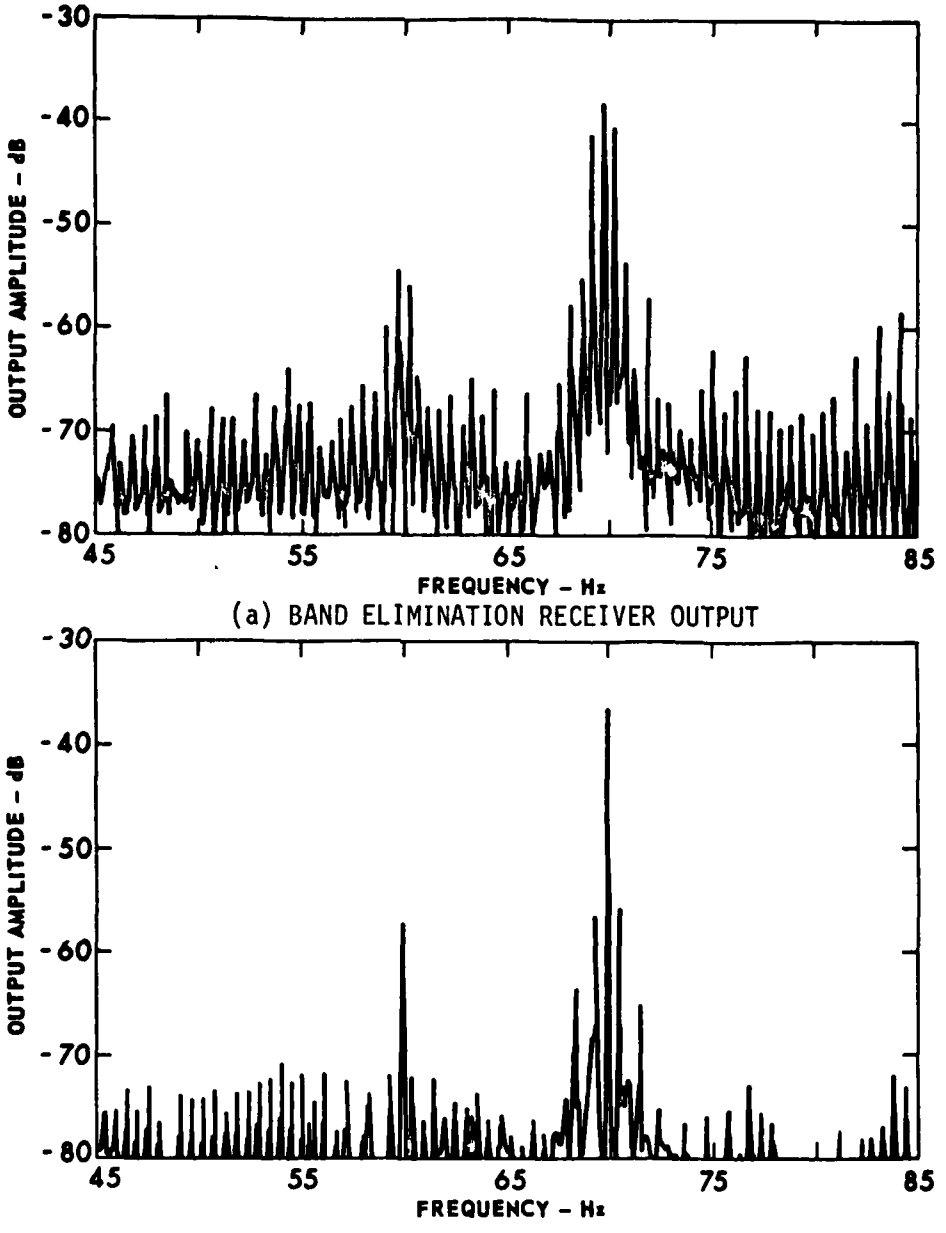

Figure. 15. Comparison of performance of band elimination and phase locked loop receivers with large amplitude transducer vibration. A 70 Hz acoustic signal was being received while the hydrophone was vibrating at a frequency of 0.53 Hz and a peak displacement of 4 mm.

REFERENCES

1. Berktay, H. O.: 1967, "Some Finite Amplitude Effects in Underwater Acoustics," in Underwater Acoustics, Vol. II (V. M. Albers, Ed.), Plenum Press.
2. Mellen, R. H., and Browning, D. G.: 1968, "Finite Amplitude Underwater Sound Propagation," in Proceedings of the NATO Advanced Study Institute on Signal Processing with Emphasis on Underwater Acoustics, (E. W. Groneveld, Ed.), Enschede, The Netherlands.
3. Berktay, H. O.: 1973, "Nonlinear Acoustics," in Signal Processing, Proceedings of the NATO Advanced Study Institute held at Loughborough, England. (J. W. R. Griffiths, P. L. Stocklin, and C. Van Schooneveld, Eds.) Academic Press.
4. Bjørnø, L.: 1977, "Parametric Acoustic Arrays," in Aspects of Signal Processing, Part 1, Proceedings of the 1976 NATO Advanced Study Institute, Portovenere, Italy (G. Tacconi, Ed.), Reidel Publishing Co.
5. Muir, T. G.: 1976, "Nonlinear Acoustics: A New Dimension in Underwater Sound," in Science, Technology and the Modern Navy, (E. I. Salkovitz, Ed.) U.S. Government Printing Office, 1977 0-242-122.
6. Westervelt, P. J.: 1963, J. Acoust. Soc. Am. 35, pp. 535-537.
7. Urick, R. J.: 1967, Principles of Underwater Sound for Engineers, McGraw-Hill Book Co., Inc.
8. Roderick, W. I.: 1976, "Bistatic Reverberation from the Sea Surface," in "Recent Developments in Underwater Acoustics," Proceedings of the AUWE Meeting, Portland, England, (British) Institute of Acoustics.
9. Lockwood, J. C., Muir, T. G., and Blackstock, D. T.: 1973, J. Acoust. Soc. Am. 53, pp. 1148-1153.
10. Muir, T. G., and Blue, J. E.: 1970, "Transient Response of the Parametric Acoustic Array," in Nonlinear Acoustics, Proceedings of the 1969 Symposium at Applied Research Laboratories (T. G. Muir, Ed.), Applied Research Laboratories, The University of Texas at Austin.
11. Jensen, F. B., and Kuperman, W. A.: 1980, "Optimum Frequency in Ducted Propagation," Proceedings 10th Intl. Congress on Acoustics, Sydney, Australia.
12. Brown, B. M.: 1970, "Sonar Signal Processing," in Underwater Acoustics (by Leon Camp, principal author) Wiley-Interscience Press.
13. Laval, R.: 1974, "Various Concepts for Future Sonars in Shallow Water," in "Sound Propagation in Shallow Water," Vol. II, Proceedings of the 1974 SACLANTCEN Conference (O. F. Hastings and O. V. Olesen, Eds.), SACLANT ASW Research Centre.
14. Truchard, J. J.: 1975, J. Acoust. Soc. Am. 58, pp. 1141-1150.
15. Zverev, V. A., and Kalachev, Z. I.: 1970, Soviet Phys.-Acoust. 16, pp. 204-208.

16. Goldsberry, T. G.: 1974, J. Acoust. Soc. Am. 56, p. S41(A). (Paper in Ref. 18.)
17. Goldsberry, T. G.: 1975, J. Acoust. Soc. Am. 57, p. S74(A). (Paper in Ref. 18.)
18. Goldsberry, T. G., Olsen, W. S., Reeves, C. R., Rohde, D. F., and Widener, M. W.: 1979, "PARRAY Technology Papers Presented at Scientific and Technical Meetings," Applied Research Laboratories Technical Report No. 79-4, Applied Research Laboratories, The University of Texas at Austin. AD A077 726.
19. Goldsberry, T. G.: 1979, "The PARRAY as an Acoustic Sensor," in Proceedings of the Conference on Underwater Applications of Nonlinear Acoustics, (British) Institute of Acoustics, University of Bath, England.
20. Berktay, H. O., and Shooter, J. A.: 1973, J. Acoust. Soc. Am. 54, pp. 1056-1061.
21. Berktay, H. O., and Muir, T. G.: 1973, J. Acoust. Soc. Am. 53, pp. 1377-1383.
22. Barnard, G. R., Willette, J. G., Truchard, J. J., and Shooter, J. A.: 1972, J. Acoust. Soc. Am. 52, pp. 1437-1441.
23. Goldsberry, et al.: 1979, "Development and Evaluation of an Experimental Parametric Acoustic Receiving Array," Applied Research Laboratories Technical Report 79-5, Applied Research Laboratories, The University of Texas at Austin. AD A072 307.
24. Rohde, D.F., Goldsberry, T. G., Olsen, W. S., and Reeves, C. R.: 1979, J. Acoust. Soc. Am. 66, pp. 484-487.
25, Reeves, C. R., Goldsberry, T. G., Olsen, W. S., and Rohde, D. F.: 1976, J. Acoust. Soc. Am. 60, p. S53(A). (Paper in Ref. 18.)
26. Reeves, C. R., Goldsberry, T. G., Rohde, D. F., and Maki, V. E., Jr.: 1980, J. Acoust. Soc. Am. 67, pp. 1495-1501.
27. Lamb, R. A.: 1980, "Investigation of a Phase-locked Loop Receiver for a Parametric Acoustic Receiving Array," Applied Research Laboratories Technical Report No. 80-25, Applied Research Laboratories, The University of Texas at Austin.

7 July 1980

DISTRIBUTION LIST FOR
ARL-TR-80-38
UNDER CONTRACT N00014-75-C-0161

Copy No.

Office of Naval Research
Department of the Navy
Arlington, VA 22217

1 - 2 Attn: R. Obrochta, Code 464
3 CAPT W. Boyer, Code 200
4 R. Winokur, Code 102C

Commander
Naval Sea Systems Command
Department of the Navy
Washington, DC 20362

5 Attn: E. Liszka, Code 63R1
6 D. Porter, Code 63R3
7 F. Romano, Code 63R3
8 A. W. Bradley, Code 63X14
9 CAPT. P. Wright, Code PMS 407
10 CDR. J. Post, Code PMS 407
11 C. Taylor, Code 05H3
12 N. G. Jenkins, Code 63X32
13 CAPT R. H. Scales, PMS 402
14 Mr. D. L. Baird, Code 63X3
15 CDR D. F. Bolka, Code 63G
16 Mr. D. M. Early, Code 63D
17 Mr. John Neely, Code 63X3

Commander
Naval Electronic Systems Command
Department of the Navy
Washington, DC 20360

18 Attn: CAPT H. Cox, PME 124
19 Dr. J. A. Sinsky, Code 320A

Defense Advanced Research Projects Agency
1400 Wilson Boulevard
Arlington, VA 22209

20 Attn: CDR V. P. Simmons
21 Dr. T. Kooij

Copy No.

Commander
Naval Material Command
Department of the Navy
Washington, DC 20360
22 Attn: CAPT O'Keefe, Code 08TB
23 T. Horwath, Code 08TC
24 CDR Young, Code 08D13
25 G. Spaulding, Code 08T23
26 J. Probus, Code 08L

Commander
Naval Air Systems Command
Washington, DC 20361
27 Attn: W. Emshwiller, Code 548C2
28 D. Rosso, Code 370

Office of the Chief of Naval Operations
Department of the Navy
Washington, DC 20350
29 Attn: CAPT L. Sykes, Code OP-374
30 D. Bradley, Code OP-374
31 CDR Hendrickson, Code OP-981D
32 CAPT Keathley, Code OP-954
33 CAPT W. Christensen, Code OP-951F
34 CAPT R. B. Gilchrist, OP-95T
35 CAPT J. Van Metre, Code OP-224
36 LCDR J. Carter, Code OP-961C4
37 CDR Harlett, Code OP-952D1
38 CDR Kelley
39 Ms. J. C. Bertrand

Office of the Chief of Naval Operations
Long Range Planning Group
2000 North Beauregard St.
Alexandria, VA 22311
40 Attn: CAPT J. R. Seesholtz, Code 00X1

Director
Naval Research Laboratory
Department of the Navy
Washington, DC 20375
41 Attn: J. Munson, Code 5100
42 F. Ingenito, Code 5120
43 W. Newbauer, Code 5108
44 L. Dragonette
45 M. Potosky, Code 5109
46 J. Jarznski, Code 5131
47 R. D. Corsaro, Code 5131

Copy No.

Commander
Naval Ship Weapon Systems Engineering Station
Department of the Navy
Port Hueneme, CA 93043
48 Attn: Dr. G. Hetland, Jr.

Naval Research Laboratory
Underwater Sound Reference Division
P. O. Box 8337
Orlando, FL 32856
49 Attn: J. E. Blue
50 A. L. Van Buren
51 P. H. Rogers

Commander
Naval Coastal Systems Center
Department of the Navy
Panama City, FL 32407
52 Attn: H. Warner, Code 791
53 D. Skinner, Code 791
54 M. Lacey, Code 720
55 J. Hammond, Code 722
56 D. Folds

Officer-in-Charge
New London Laboratory
Naval Underwater Systems Center
Department of the Navy
New London, CT 06320
57 Attn: M. Moffett
58 R. H. Mellen
59 W. Konrad
60 R. Schumaker
61 L. King

Commanding Officer
Naval Surface Weapons Center
White Oak Laboratory
Department of the Navy
Silver Spring, MD 20910
62 Attn: G. Gaunaurd, Code R31
63 G. Kalaf, Code U5

Commander
Naval Ocean Systems Center
Department of the Navy
San Diego, CA 92152
64 Attn: H. Bucker, Code 5311
65 F. Gordon, Code 633
66 J. Reeves, Code 635
67 W. Angeloff, Code 6233

Copy No.

Commanding Officer
Naval Ocean Research and Development Activity
NSTL Station, MS 39529
68 Attn: R. Goodman, Code 110
69 S. Marshal, Code 340
70 J. Posey, Code 340
71 Mr. Soloman, Code 500
72 A. L. Anderson, Code 320

73 Commander
Naval Intelligence Command
2461 Eisenhower Avenue
Alexandria, VA 22331

Commander
Naval Explosive Ordnance Disposal Facility
Indian Head, MD 20640
74 Attn: Mr. L. H. Dickinson, Technical Director

Commanding Officer
USCG Research and Development Center
Avery Point
Groton, CT 06340
75 Attn: CAPT M. Y. Suzich

Officer-in-Charge
David W. Taylor Naval Ship Research and Development Center
Department of the Navy
Bethesda, MD 20084
76 Attn: R. Rippeon

National Academy of Sciences
Naval Studies Board
2101 Constitution Avenue, NW
Washington, DC 20418
77 Attn: L. Hunt

Commanding Officer
Naval Postgraduate School
Monterey, CA 93940
78 Attn: Prof. G. Sacklman
79 Prof. A. B. Coppens
80 Prof. J. V. Sanders

Copy No.

North Atlantic Treaty Organization
SACLANT ASW Research Centre
APO 09019
New York, NY
81 Attn: W. Kuperman
82 F. Whicker
83 F. Jensen

Applied Research Laboratory
The Pennsylvania State University
Post Office Box 30
State College, PA 16801
84 Attn: F. H. Fenlon

The Catholic University of America
Washington, DC 20064
85 Attn: Dr. Überall

Westinghouse Electric Corporation
P. O. Box 1488
Annapolis, MD 21404
86 Attn: Mr. A. Nelkin
87 Dr. P. J. Welton

Raytheon Company
P. O. Box 360
Portsmouth, RI 02871
88 Attn: Mr. J. F. Bartram

89 Mr. E. P. Aurand
19 Hanapepe Place
Honolulu, HI 96825

Department of Engineering and Applied Science
Yale University
New Haven, CT 06520
90 Attn: Dr. P. M. Schultheiss

RAMCOR, Inc.
800 Follin Lane
Vienna, VA 22180
91 Attn: Mr. V. J. Lujetic

Systems Planning Corporation
1500 Wilson Blvd., Suite 1500
Arlington, VA 22209
92 Attn: Mr. Jack Fagan

Copy No.

Bolt, Beranek & Newman, Inc.
50 Moulton Street
Cambridge, MA 02138
93 Attn: Dr. J. E. Barger
94 Dr. F. J. Jackson

Scripps Institution of Oceanography
Marine Physical Laboratory
University of California
San Diego, CA 92152
95 Attn: Dr. William S. Hodgkiss

Tracor, Inc.
6500 Tracor Lane
Austin, TX 78721
96 Attn: Mr. J. D. Williams
97 Mr. J. Dow

Radian Corporation
8500 Shoal Creek Blvd.
P. O. Box 9948
Austin, TX 78757
98 Attn: Mr. Jerry L. Bardin
99 Dr. C. R. Reeves

General Physics Corporation
10630 Little Patuxent Parkway
Columbia, MD 21044
100 Attn: Dr. Frank Andrews

Trans World Systems, Inc.
1311A Dolly Madison Blvd.
McLean, VA 22101
101 Attn: Mr. Sam Francis

102-113 Commanding Officer and Director
Defense Technical Information Center
Cameron Station, Building 5
5010 Duke Street
Alexandria, VA 22314

Battelle Memorial Institute
505 King Avenue
Columbus, OH 43201
114 Attn: TACTEC

Distribution List for ARL-TR-80-38 under Contract N00014-75-C-0161 (Cont'd)

Copy No.

115	Office of Naval Research Resident Representative Room 582, Federal Building Austin, TX 78701
116	Physical Acoustics Group, ARL:UT
117	Garland R. Barnard, ARL:UT
118	C. Robert Culbertson, ARL:UT
119	Tommy G. Goldsberry, ARL:UT
120	Loyd Hampton, ARL:UT
121	John M. Huckabay, ARL:UT
122	Robert A. Lamb, ARL:UT
123	T. G. Muir, ARL:UT
124	David F. Rohde, ARL:UT
125	Reuben H. Wallace, ARL:UT
126	Library, ARL:UT
127-136	ARL:UT Reserve